Acta Cryst. (1994). B50, 663–672

Oxygen-Induced Structural Change of the Tetragonal Phase Around the Tetragonal–Cubic Phase Boundary in ZrO_2–$YO_{1.5}$ Solid Solutions

BY MASATOMO YASHIMA, SATOSHI SASAKI AND MASATO KAKIHANA

Research Laboratory of Engineering Materials, Tokyo Institute of Technology, 4259 *Nagatsuta, Midori-ku, Yokohama* 227, *Japan*

YASUO YAMAGUCHI

Research Institute for Materials, Tohoku University, 2-1-1 *Katahira, Sendai* 980, *Japan*

HARUO ARASHI

Department of Machine Intelligence and Systems Engineering, Faculty of Engineering, Tohoku University, Aramaki-Aza-Aoba, Aoba-ku, Sendai 980, *Japan*

AND MASAHIRO YOSHIMURA

Research Laboratory of Engineering Materials, Tokyo Institute of Technology, 4259 *Nagatsuta, Midori-ku, Yokohama* 227, *Japan*

(*Received* 8 *November* 1993; *accepted* 2 *June* 1994)

Abstract

In the ZrO_2–$YO_{1.5}$ solid solutions, the phase changes among the cubic phase (*Fm*3*m*, $Z = 4$), the *t*″ form and the *t*′ form were investigated by neutron and X-ray powder diffraction, where the *t*″ and *t*′ forms are defined as tetragonal phases ($P4_2/nmc$, $Z = 2$) with axial ratios of $c/a_f = 1$ and $c/a_f > 1$, respectively, which were prepared by a diffusionless transition from the high-temperature cubic phase during quenching. a_f is the lattice parameter of the pseudo-fluorite cell. The crystal structure of the tetragonal phase of $Zr_{1-X}Y_XO_{2-X/2}$ [$= (ZrO_2)_{1-X}(YO_{1.5})_X$; $X =$ 0.10, 0.12, 0.14 and 0.16] has been refined both by the direct estimation of the integrated intensity ratio $I(102)/I(101)$ and by the Rietveld analysis of neutron powder diffraction data collected at 293 K [$\lambda =$ 1.5301 (3) or 1.5314 (2) Å]. The crystal structure of $Zr_{1-X}Y_XO_{2-X/2}$ ($X = 0.18$ and 0.20) has also been refined assuming either tetragonal ($P4_2/nmc$, $Z = 2$) or cubic symmetry [*Fm*3*m*, $Z = 4$] by the Rietveld analysis of neutron powder diffraction data collected at 293 K [$\lambda = 1.5301$ (3) Å]. The lattice parameters were determined by profile-fittings of Cu $K\alpha$ X-ray powder diffraction data. The oxygen displacement from the ideal anion coordinate of the cubic fluorite-type structure, $0.25 - z$, decreased with an increase of $YO_{1.5}$ content, where z is the atomic coordinate of oxygen. The axial ratio c/a_f also decreased with an increase of $YO_{1.5}$ content. The $Zr_{0.84}Y_{0.16}O_{1.92}$ sample, whose axial ratio c/a_f is equal to unity within experimental error, has clearly exhibited oxygen displacement along the *c* axis from the ideal site (8*c*) of the fluorite-type structure (*t*″ form). The space group of the *t*″ form was finally assigned to be $P4_2/nmc$ after the examination of various space groups which are subgroups of *Fm*3*m* and supergroups of $P4_2/nmc$. The coexistence of the *t*′ and *t*″ forms in the $Zr_{0.86}Y_{0.14}O_{1.93}$ sample suggests the existence of an energy barrier between them and that the high-temperature cubic phase transforms into the *t*″ form and then a part of the *t*″ form transforms into the *t*′ form.

Introduction

The excellent mechanical and electrical properties of zirconia ceramics strongly depend on the crystal structures and the phase changes, which should be described by a temperature–composition metastable–stable phase diagram shown in Fig. 1 (Yashima, Ishizawa & Yoshimura, 1993*a*–*c*). The stable phase diagrams have been investigated extensively by numerous researchers. However, there are still numerous discrepancies, misunderstandings and contradictions among them. One of the most important keys to solve these problems is the investigation of the diffusionless cubic–tetragonal phase transition (Yoshimura, 1988; Heuer, Chaim & Lanteri, 1989; Yashima *et al.*, 1993*a*–*c*; Sakuma, 1993).

Pure zirconia (zirconium dioxide, ZrO_2) has three solid polymorphs of monoclinic [$P2_1/c$, $Z = 4$ (McCullough & Trueblood, 1959; Smith & Newkirk,

1965)], tetragonal [$P4_2/nmc$, $Z=2$ (Teufer, 1962)] and cubic [$Fm3m$, $Z=4$ (Smith & Cline, 1962)] symmetries at atmospheric pressure

monoclinic ⟷ tetragonal ⟷ cubic ⟷ liquid

1443 K 2643 K 2953 K

(Subbarao, 1981).

The tetragonal structure is derived from the fluorite-type structure both by the elongation of one of the three equal crystallographic axes of the cubic fluorite structure with respect to the other two (Lefevre, Collongues & Perez y Jorba, 1959) and by the shift of the oxygen ion from its ideal position in the fluorite structure (arrows in Fig. 2; Teufer, 1962; Barker, Bailey & Garrett, 1973; Michel, Mazerolles & Perez y Jorba, 1983).

The high-temperature tetragonal and cubic phases can generally be stabilized to room temperature by doping such oxides as $YO_{1.5}$, $ErO_{1.5}$ and CeO_2. The behavior of the cubic-tetragonal phase transition in the oxide-doped zirconia is very interesting, because the doped tetragonal zirconia is classified into three forms and the transformations among them are very complicated (Yashima *et al.*, 1993*a–c*). The tetragonal phase with the dopant composition of X_t precipitates through a diffusional phase separation, when the sample is annealed within the (tetragonal + cubic) two-phase region of the phase diagram in the ZrO_2–$YO_{1.5}$ system (A in Fig. 1). This tetragonal phase formed diffusionally is called the t form. As shown by path B in Fig. 1, another tetragonal form is formed through a diffusionless phase transition from the cubic phase at or below the equilibrium temperature T_0^{c-t} between the cubic and tetragonal phases when the high-temperature cubic phase is quenched to room temperature (Scott, 1975; Heuer, Chaim & Lanteri, 1987). At T_0^{c-t}, the Gibbs free energy of the tetragonal phase is assumed to be identical to that of the cubic. This tetragonal phase formed diffusionlessly is called the t' form to distinguish it from the t form (Miller, Smialek & Garlick, 1981). The $c \rightarrow t'$ phase transition has been extensively studied by many researchers (for example, Yashima *et al.*, 1993*a–c*; Sakuma, 1993). The t' form shows a characteristic domain structure (Michel *et al.*, 1983). The $c \rightarrow t'$ phase transition has been suggested to be accompanied by the oxygen displacement from the ideal fluorite site. However, the displacement values in the vicinity of the tetragonal–cubic phase boundary and its compositional depen-

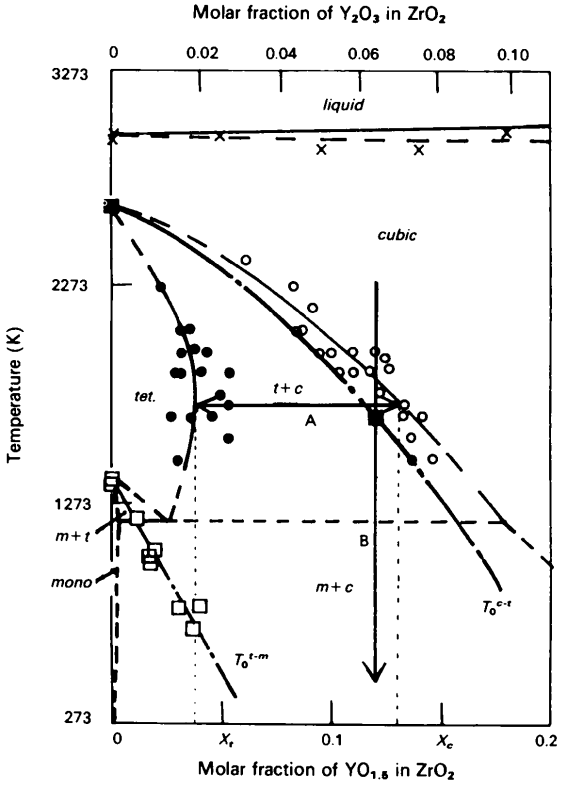

Fig. 1. Temperature–composition metastable–stable phase diagram of the ZrO_2-rich part in the ZrO_2–$YO_{1.5}$ system after Yashima *et al.* (1993*c*). Experimental data for stable phase boundaries (———— established and ---------- not established): × the solidification temperature, ● the tetragonal/(tetragonal + cubic) phase boundary, and ○ the (tetragonal + cubic)/cubic phase boundary. Experimental data for metastable phase boundaries — — — —: ■ the equilibrium temperature T_0^{c-t} between cubic and tetragonal phases, and □ the equilibrium temperature T_0^{t-m} between tetragonal and monoclinic phases.

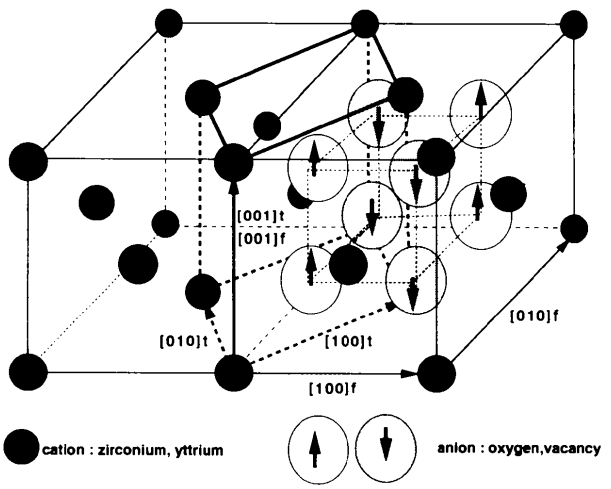

Fig. 2. Crystal structure of tetragonal zirconia and relationship between tetragonal (t) cell and pseudo-fluorite (f) cell. The solid circles are the cations. The open circles are the anions with the displacement from their ideal fluorite lattice sites in upper directions. The hatched circles are the anions with the displacement from their ideal fluorite lattice sites in downward directions. Heavy lines indicate a primitive cell after Teufer (1962) and light lines delineate two pseudo-fluorite cells.

dence is not known yet. Yashima, Ohtake, Arashi, Kakihana & Yoshimura (1993) studied the tetragonal–cubic phase boundary using Raman scattering. It has been suggested that the oxygen displacement decreases with an increase of the $YO_{1.5}$ content (Zhou, Lei & Sakuma, 1991; Sato, Yashima, Yoshimura & Toraya, 1991) and that the cubic-to-tetragonal phase transition is induced not by the lattice change but by oxygen displacements along the c axis from the ideal anion site in the fluorite-type cubic phase (8c) (Sugiyama & Kubo, 1986; Yashima *et al.*, 1993*a*). The X-ray diffraction technique is not sensitive enough in zirconia ceramics to observe the cubic–tetragonal phase change because of the relatively small atomic scattering factor of oxygen. It is difficult for the electron-diffraction and Raman scattering to quantify the oxygen-displacement value, which is very important for the quantitative discussion of the cubic–tetragonal phase transition using an order parameter (η in Fig. 3; Hillert & Sakuma, 1991; Yashima & Yoshimura, 1992; Yashima *et al.*, 1993*a–c*). Therefore, neutron diffraction was used both to quantify the oxygen displacement and to investigate directly the oxygen-induced structural change with the help of the relatively large scattering length of oxygen. In the present study we focus our attention on the structural change around the cubic–tetragonal phase boundary in the ZrO_2–$YO_{1.5}$ system using neutron and X-ray powder diffraction.

There is another tetragonal form, the t'' form defined as a tetragonal form with an axial ratio c/a_f of unity but with an oxygen displacement along the c axis from the 8c site of the fluorite-type structure, where the a_f is a lattice parameter of the pseudo-fluorite cell (Sugiyama & Kubo, 1986; Yashima *et al.*, 1993*a,c*). According to high-temperature X-ray diffraction studies (Yashima *et al.*, 1993*a,c*), a part of the t'' form discontinuously changes into the t' form with an axial ratio $c/a_f > 1$ and the fraction of the t' form increases with annealing time, suggesting that there is an energy barrier between the two forms (ΔG^* in Fig. 3). Therefore, the t'' form was distinguished from the t' form, although both forms were assumed to have the same space group of $P4_2/nmc$ in previous work (Yashima *et al.*, 1993*a*). In the present study we will also assign the space group of the t'' form to confirm this assumption.

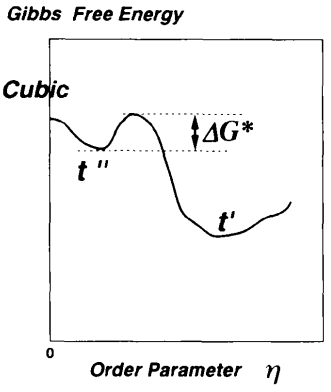

Fig. 3. Schematic free energy–order parameter curve at a temperature (*e.g.* 1073 K) below the equilibrium temperature T_0^{c-t} between tetragonal and cubic phases. This curve was originally proposed to explain the transformation behavior in the rapidly quenched $Zr_{0.86}R_{0.14}O_{1.93}$ solid solutions (R = Er and Y; Yashima *et al.*, 1993*a,c*).

Sample preparation

The samples used for data collection were all prepared from commercially available zirconia, containing a small amount of hafnia which comes from the raw material (hafnium dioxide, HfO_2, 1.98 wt% in ZrO_2). The starting materials were high-purity zirconia [Tosoh Co. Ltd., Tokyo, Japan 99.9% (97.9 wt% ZrO_2 + 1.98 wt% HfO_2), grade UPZ-200] and yttria (Shin-Etsu Chemicals Co. Ltd., Tokyo, Japan, 99.99%) powders. They were manually mixed as methanol slurries or dried powders with a pestle in an agate mortar for 3 h. The mixed powder was pressed into pellets (20 mm in diameter and 10–20 mm in height) by hand and then isostatically pressed at *ca* 200 MPa. The pellets were fired at 1673 K in air for 5 h in an electric furnace. The fired product was crushed and ground in an alumina mortar for 2 h and then pressed again into pellets at about 200 MPa. $Zr_{1-X}Y_XO_{2-X/2}$ samples (X = 0.10, 0.12 and 0.14) were then fired at 2173 (±100) K in air in an electric furnace with stabilized zirconia heaters to homogenize the $YO_{1.5}$ contents and then quenched by being dropped into water to obtain compositionally homogeneous samples without the (tetragonal + cubic) phase separation (B in Fig. 1). While the $Zr_{1-X}Y_XO_{2-X/2}$ samples for X = 0.16, 0.18, 0.20 and 0.22 were fired at 1973 K in air in an electric furnace with $MoSi_2$ heaters to homogenize the $YO_{1.5}$ contents (Fig. 1) and then cooled with a cooling rate of 10 K min^{-1}. Sintered materials were crushed again into powders in an alumina mortar to measure the powder diffraction.

X-ray diffraction data collection and refinement

The X-ray powder diffraction method was used to determine the lattice parameter of the samples. Each sample was mixed well with an internal Si-powder standard (a_0 = 5.43094 Å, 99.999%) for angular calibration. The X-ray diffraction profiles of the mixed samples were collected with an X-ray diffractometer (MXP^{3VA}, MAC Science Co. Ltd., Tokyo, Japan) under the following experimental conditions: tube

generated Cu $K\alpha$ radiation; curved graphite diffracted-beam monochromator; goniometer radius = 185 mm; divergence slit = 1°; anti-scatter slit = 1°; receiving slit = 0.15 mm; NaI (Tl) scintillation counter; step-scan mode; step width = 0.02° in 2θ; fixed time = 5 s; 2θ range = 68–150°. Individual profile fits were performed for the powder data using a profile-fitting program *PRO-FIT* (Toraya, 1986, 1993). The peaks were fitted with a Pearson VII-type function. The lattice parameters of the samples were calculated using the least-squares program *RLC*3 (Sakurai, 1985). Also, the least-squares program attached to the Mac Science MXP system gave the same lattice parameters.

Neutron diffraction data collection and refinement

The powders were contained in a 10 mm $\phi \times 50$ mm vanadium can for the data collection of neutron diffraction. Neutron diffraction data for all samples were collected at 293 K on a single-counter fixed-wavelength powder diffractometer (KPD) at the JRR-3M research reactor of Japan Atomic Energy Research Institute, Tokai Research Laboratories (Funahashi, Ito & Yoshizawa, 1991). A neutron beam was monochromatized by the (311) plane of a Ge monochromator. The profile data were measured by scanning at intervals of 0.10° in the 2θ range shown in Table 1, where the fixed time was 1 min.

Individual profile fits were performed assuming a Gaussian function. Using observed peak positions $2\theta_{obs}$ in the neutron diffraction patterns and the lattice parameters obtained from X-ray diffraction data (Table 2), the neutron wavelength λ was determined by Bragg's equation $\lambda = 2d\sin(\theta_{obs} + \Delta\theta)$, where d is the plane distance and $\Delta\theta$ is the zero point shift. The plots of $2d\cos\theta_{obs}$ *versus* $2d\sin\theta_{obs}$ were used to determine λ by the equation

$$\lambda = 2d\sin\theta_{obs} + \Delta\theta\, 2d\cos\theta_{obs}.$$

Refined wavelengths are shown in Table 1. Data collection was carried out in two series of machine times with two wavelengths, 1.5301 (3) and 1.5314 (2) Å for each.

The oxygen atomic coordinate z of the tetragonal phase was estimated by two methods. One method is a direct estimation from the integrated intensity ratio $I(102)/I(101)$. The neutron diffraction data were collected around the 101 and 102 reflections, where the fixed times for 102 reflection measurements are shown in the bottom of Table 3. Individual profile fits of 102 and 101 reflections were performed assuming a Gaussian function. z was calculated from $I(102)/I(101)$ by the following equation

$$z = (1/4 - 1/4\pi)\sin^{-1}[(b_c/b_a) \times \{[I(102)\,L(101)]/[I(101)\,L(102)]\}^{1/2}],$$

where b_c and b_a are the average neutron scattering lengths of cation and anion containing vacancy, $I(hkl)$ and $L(hkl)$ are the integrated intensity and Lorentz factor for hkl reflections, respectively (Yashima *et al.*, 1993*b*; Yashima, Morimoto, Ishizawa & Yoshimura, 1993). The other is the least-squares refinements of structure and total profile. The calculations were performed by a Rietveld analysis program *RIETAN* (Izumi, 1985, 1993) with the following scattering lengths: Zr, 7.160; Hf, 7.770; Y, 7.750; O, 5.805 fm. The peak shape was assumed to be a modified pseudo-Voigt function with asymmetry. The neutron diffraction pattern indicated a characteristic background because of the diffuse scattering (Steele & Fender, 1974; Martin, Boysen & Frey, 1993). Therefore, we conducted the Rietveld refinement by two methods. In one method, the background of each profile was approximated by a six-parameter polynomial in $2\theta^n$, where n has values between 0 and 5. The n parameters were simultaneously refined with the unit-cell, zero-point, scale, peak-width/shape/asymmetry and crystal structural parameters. In the other method, the characteristic background was subtracted before the Rietveld refinement, assuming a seven-parameter polynomial in $2\theta^n$ where n has values between 0 and 6.

Results and discussion

The X-ray diffraction patterns in Fig. 4 indicate that the samples for composition $X = 0.10$ and 0.12 are a single t'-form and the 004 and 220 reflections split into two peaks due to the difference in a_f and c_{tet} values, where $a_f = (2)^{1/2} a_{tet}$ (Teufer, 1962; Aldebert & Traverse, 1985; Yashima *et al.*, 1993*b*). The samples for $X \geq 0.16$ are the t'' form or cubic without the splitting between 004 and 220 reflections. The sample with the composition $X = 0.14$ is identified as a mixture of t' and t'' forms, as shown in Fig. 4(*c*). The profile-fitting is successfully performed assuming that there are three peaks of (1) the 004 reflection of the t' form $004_{t'}$, (2) $004_{t'} + 220_{t'}$, and (3) $220_{t'}$. The lengths of a_f and c axes increase and decrease, respectively, with an increase of $YO_{1.5}$ content X in the region between $X = 0.10$ and 0.14 (Table 2 and Fig. 5). In the compositional region of $X \geq 0.14$, the two axes become identical and increase with an increase of $YO_{1.5}$ content.

As shown in Fig. 6, the peak intensity of the 102_{tet} reflection, which is equivalent to 112_f that is forbidden for the fluorite-type structure, decreases with an increase of $YO_{1.5}$ content. This indicates that the oxygen displacement from the 8*c* site of the fluorite-type cubic structure becomes smaller with the $YO_{1.5}$ content. In the $Zr_{0.82}Y_{0.18}O_{1.91}$ and $Zr_{0.80}Y_{0.20}O_{1.90}$ samples, the 102_{tet} peak could not be observed beyond the experimental errors. However, it should

Table 1. *Summary of neutron diffraction data collection and refinement for* ZrO_2–$YO_{1.5}$

X of $Zr_{1-x}Y_xO_{2-x/2}$	0.10	0.12	0.14	0.16	0.18	0.18	0.20	0.20
Space group	$P4_2/nmc$	$P4_2/nmc$	$P4_2/nmc$	$P4_2/nmc$	$P4_2/nmc$	$Fm3m$	$P4_2/nmc$	$Fm3m$
2θ scan range (°)	27–94.9	25–94.9	27–97	27–97	25–94.9	25–94.9	27–94.9	27–94.9
Wavelength (Å)	1.5301 (3)	1.5314 (2)	1.5314 (2)	1.5314 (2)	1.5301 (3)	1.5301 (3)	1.5301 (3)	1.5301 (3)
Maximum step intensity (min)	2935	2810	2854	2765	3968	3968	3211	3211
No. of unique reflections	24	24	24	24	24	9	24	9
No. of structural parameters	3	3	5	3	3	2	3	2
No. of profile parameters	14	14	14	14	14	14	14	14
R_{wp} (%)*†	6.84	16.27	13.18	16.86	13.12	13.40	9.68	9.52
R_e (%)*†	5.77	11.88	10.59	12.16	7.86	7.87	7.05	7.06
GoF*†	1.19	1.37	1.24	1.39	1.67	1.70	1.37	1.35
R_B (%)*†	3.38	5.09	5.29	5.69	5.95	4.33	4.22	2.98
R_{wp} (%)*‡	6.61	16.13	12.77	16.14	11.09	11.18	8.65	8.67
R_e (%)*‡	5.75	11.95	10.59	12.22	7.87	7.88	7.05	7.05
GoF*‡	1.15	1.35	1.21	1.32	1.41	1.42	1.22	1.23
R_B (%)*‡	2.97	4.56	4.75	5.67	3.45	3.02	3.11	2.39

* Standard Rietveld analysis agreement index (Young, Prince & Sparks, 1982).

† Background of each profile was approximated by a six-parameter polynominal in $2\theta^n$ and refined during the Rietveld analysis.

‡ Background was subtracted before the Rietveld refinement assuming a seven-parameter polynominal in $2\theta^n$, where n had values between 0 and 6.

Table 2. *Cell parameters refined using the X-ray diffraction data*

X of $Zr_{1-x}Y_xO_{2-x/2}$	0.10	0.12	0.14	0.16	0.18	0.20	0.22
a (Å) (tetragonal)	3.6183 (5)	3.6228 (1)	3.6258				
c (Å) (tetragonal)	5.1634 (1)	5.1575 (2)	5.1514				
a (Å) (cubic or t'')*			5.1370	5.14086 (8)	5.14335 (7)	5.14728 (9)	5.15093 (13)

* Fluorite cell parameter.

Table 3. *Cell parameters used for the refinement of neutron diffraction data and obtained fractional atomic coordinates and isotropic thermal parameters for* ZrO_2–$YO_{1.5}$

X of $Zr_{1-x}Y_xO_{2-x/2}$	0.10	0.12	0.14	0.16	0.18	0.18	0.20	0.20
Space group	$P4_2/nmc$	$P4_2/nmc$	$P4_2/nmc$	$P4_2/nmc$	$P4_2/nmc$	$Fm3m$	$P4_2/nmc$	$Fm3m$
a (Å)*	3.6183	3.6228	3.6310 (4)	3.6351	3.6369	5.14335	3.63968	5.14728
c (Å)*	5.1634	5.1575	5.1533 (10)	5.14086	5.14335	5.14335	5.14728	5.14728
Zr x	0	0	0	0	0	0	0	0
y	0	0	0	0	0	0	0	0
z	0	0	0	0	0	0	0	0
B (Å^2)*	1.0 (2)	1.0 (3)	1.1 (3)	1.2 (4)	1.0 (3)	1.0 (5)	1.1 (3)	1.1 (5)
O x	0	0	0	0	0	0.25	0	0.25
y	0.5	0.5	0.5	0.5	0.5	0.25	0.5	0.25
z*	0.217 (2)	0.223 (3)	0.230 (3)	0.236 (4)	0.238 (5)	0.25	0.239 (6)	0.25
B (Å^2)*	1.6 (2)	1.8 (3)	2.2 (3)	2.6 (4)	2.3 (4)	2.4 (6)	2.5 (3)	2.6 (5)
a (Å)†	3.6183	3.6228	3.6309 (4)	3.6351	3.6369	5.14335	3.63968	5.14728
c (Å)†	5.1634	5.1575	5.1532 (10)	5.14086	5.14335	5.14335	5.14728	5.14728
Zr x	0	0	0	0	0	0	0	0
y	0	0	0	0	0	0	0	0
z	0	0	0	0	0	0	0	0
B (Å^2)†	1.1 (2)	1.1 (3)	1.1 (3)	1.2 (3)	1.2 (2)	1.2 (4)	1.3 (2)	1.3 (4)
O x	0	0	0	0	0	0.25	0	0.25
y	0.5	0.5	0.5	0.5	0.5	0.25	0.5	0.25
z†	0.217 (2)	0.223 (3)	0.230 (3)	0.238 (4)	0.242 (5)	0.25	0.243 (7)	0.25
B (Å^2)†	1.8 (2)	1.9 (3)	2.2 (3)	2.6 (3)	2.4 (2)	2.5 (5)	2.6 (3)	2.6 (4)
O								
Integrated time (min)	12	8	13	8	9	9		
z‡	0.2129 (8)	0.2235 (14)	0.226 (4)	0.237 (3)	Not observed clearly	Not observed clearly		

* Background of each profile was approximated by a six-parameter polynominal in $2\theta^n$ and refined during the Rietveld analysis.

† Background was subtracted before the Rietveld refinement assuming a seven-parameter polynominal in $2\theta^n$, where n had values between 0 and 6.

‡ Direct estimation from the integrated intensity ratio $I(102)/I(101)$.

be emphasized that a weak Raman band at *ca* 470 cm^{-1}, which is characteristic of the tetragonal phase, is observed in the same $Zr_{0.82}Y_{0.18}O_{1.91}$ sample (Yashima *et al.*, 1993). The 102_{tet} reflection has been observed in electron-diffraction patterns for $X =$ 0.182 by Suzuki, Tanaka & Ishigame (1985), for $X =$ 0.148 by Suto, Sakuma, Yoshikawa & Higuchi (1987) and by Zhou *et al.* (1991). Faber, Mueller & Cooper (1978) observed the odd–odd–even reflections which are forbidden for the fluorite-type struc-

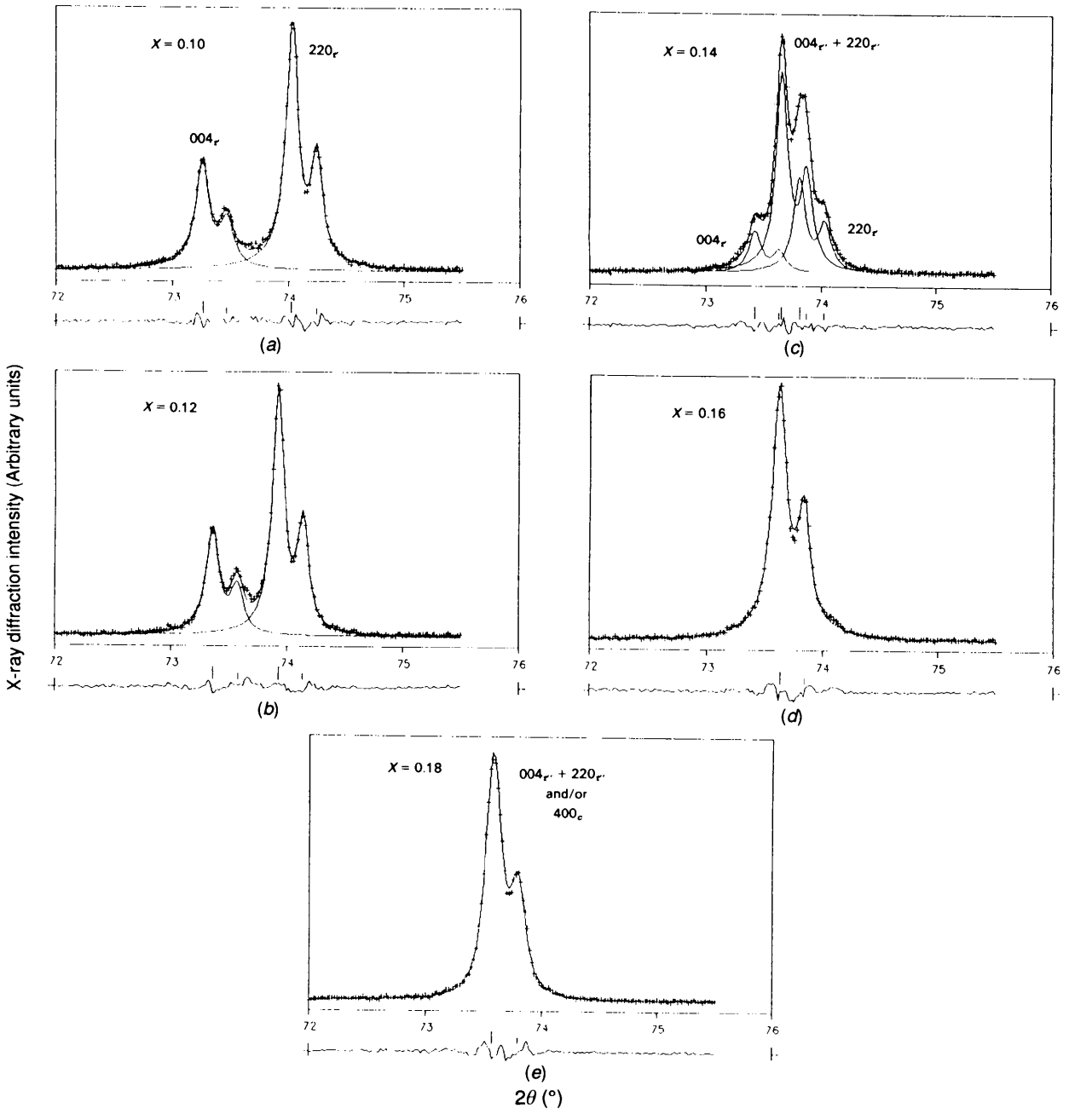

Fig. 4. Profile-fitting patterns of the sintered $Zr_{1-x}Y_xO_{2-x/2}$ samples: $X =$ (*a*) 0.10, (*b*) 0.12, (*c*) 0.14, (*d*) 0.16 and (*e*) 0.18. Observed (+) and calculated (solid line) profile intensities and their difference on the same scale, including the $K\alpha_1$ and $K\alpha_2$ splitting. The profile of the $Zr_{0.86}Y_{0.14}O_{1.93}$ sample can be made deconvolution into three peaks of (1) the 004 reflection of the *t'* form $004_{t'}$, (2) $004_{t'} + 220_{t'}$, and (3) $220_{t'}$. The reliability factor was $R_p = 3.2\%$ and $R_{wp} = 4.7\%$ ($72.5 \le 2\theta \le 75$) and defined as $R_p = \sum|y(2\theta_i)_{obs} - y(2\theta_i)_{calc}|/\sum y(2\theta_i)_{obs}$ and $R_{wp} = \sum\{w_i[y(2\theta_i)_{obs} - y(2\theta_i)_{calc}]^2\}/\sum w_i y(2\theta_i)^2_{obs}$. The volume fraction value for the *t''* form was 0.581 from $V_{t''} = [I_{t'}(004) + I_{t'}(220)]/[I_{t'}(004) + I_{t'}(220) + I_t(004) + I_t(220)]$.

ture in the neutron powder diffraction pattern for $X = 0.18$. Some researchers have observed the forbidden reflections in the sample of $X = 0.18$, although we could not detect them in the present study. The oxygen displacement may be too small to be detected by the present neutron diffraction method because of the limitation of the neutron flux, and/or that the crystallite size of the tetragonal crystal keeping the periodicity of the oxygen displacement in the present sample of $X = 0.18$ may be smaller than the coherence length. Zhou *et al.* (1991) suggested that the crystallite (domain) size decreases with an increase of $YO_{1.5}$ content. The following Rietveld analyses for the samples with $X = 0.18$ and 0.20 were, therefore, performed in two models with the tetragonal and cubic symmetries.

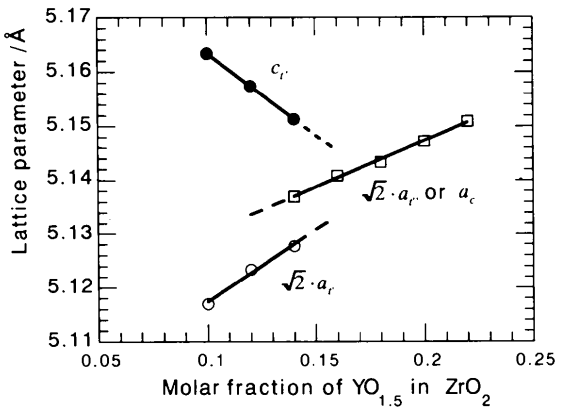

Fig. 5. Variation of the lattice parameters against the $YO_{1.5}$ contents.

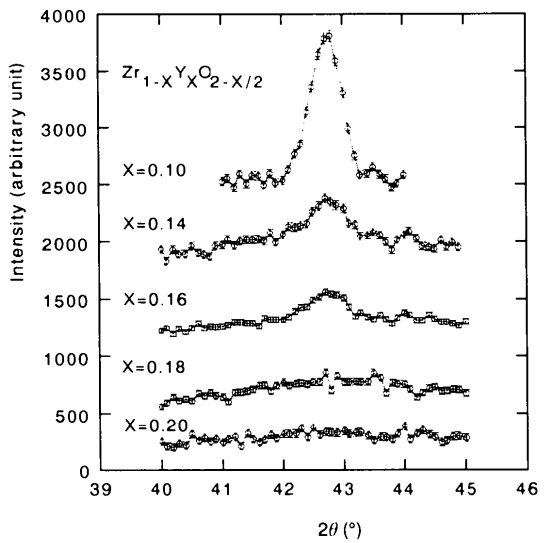

Fig. 6. The 102 reflection profiles of neutron diffraction in the ZrO_2–$YO_{1.5}$ solid solution. The backgrounds show a broad peak at *ca* 43°/2θ due to the diffuse scattering.

Table 4. *Crystal structure consideration and the space group selection having Fm3m as a supergroup and $P4_2/nmc$ as a subgroup*

Crystal system	Space group	Counter evidence
Tetragonal	*P4/mmm*	Atomic coordinates of cations
	P4/nmm	Atomic coordinates of cations
	$P4_2/mmc$	Atomic coordinates of anions
	$P4_2/mcm$	Atomic coordinates of cations
	I4/mmm	No existence of 112_f reflection observed in the diffraction pattern of the *t''* form
	I4/mcm	Atomic coordinates of cations
Cubic	*Pm-3m*	Generation of 210 and 320 reflections which are not observed in the diffraction pattern of the *t''* form

It is noteworthy that the $Zr_{0.84}Y_{0.16}O_{1.92}$ sample gave the intensity for the 102_{tet} reflection (Fig. 6) and, therefore, the oxygen displacement exists (Note, $a_f = c$ within experimental error; see Figs. 4*d* and 5 and Table 3). This tetragonal phase was conveniently assigned as the *t''* form having the space group $P4_2/nmc$ and the axial ratio $c_{tet}/a_f = c_{tet}/[(2)^{1/2}a_{tet}] = 1$ (Sugiyama & Kubo, 1986; Yashima *et al.*, 1993*a–c*). The space group of the *t''* form is confirmed to be $P4_2/nmc$ from the crystal structure consideration and the space-group selection assuming *Fm3m* as a supergroup and $P4_2/nmc$ as a subgroup (Table 4).

Rietveld analyses of the neutron powder diffraction data were performed assuming the space group $P4_2/nmc$ for $X = 0.10$–0.20 and *Fm3m* for $X = 0.18$ and 0.20. In the tetragonal structure, the cations (Zr, Y, Hf) and anion O were assumed to be located in special positions 2(*a*) and 4(*d*), respectively. The occupancies of cation and anion sites were assumed to be 1 and $1 - X/4$, respectively. The calculated profile patterns showed a good fitness with the observed ones (Fig. 7 and Table 1). Figs. 7(*a*), 7(*b*) and 7(*c*) show the neutron powder diffraction patterns of samples for $X = 0.10$, 0.16 and 0.20 refined based on the *t'*, *t''* and *c* forms, respectively. These diffraction patterns are very similar to each other, suggesting that these forms have similar crystal structures. The neutron diffraction profile for $X = 0.20$ (Fig. 7*c*) shows an ideal fluorite-type structure. Note that extra peaks forbidden for the fluorite-type structure appear for $X = 0.16$ because of the oxygen displacement (arrows in Fig. 7*b*). In the neutron diffraction profile for $X = 0.10$, some reflections are interpreted to split because of the differences in lengths between the a_f and *c* axes. However, because no difference in the lengths is present for $x = 0.16$, no splitting is interpreted to exist for the reflections with solid circles in Fig. 7(*b*).

The atomic coordinate *z* of the O atom increased linearly with an increase of $YO_{1.5}$ content in the compositional region of $0.10 \le X \le 0.16$ (Table 3

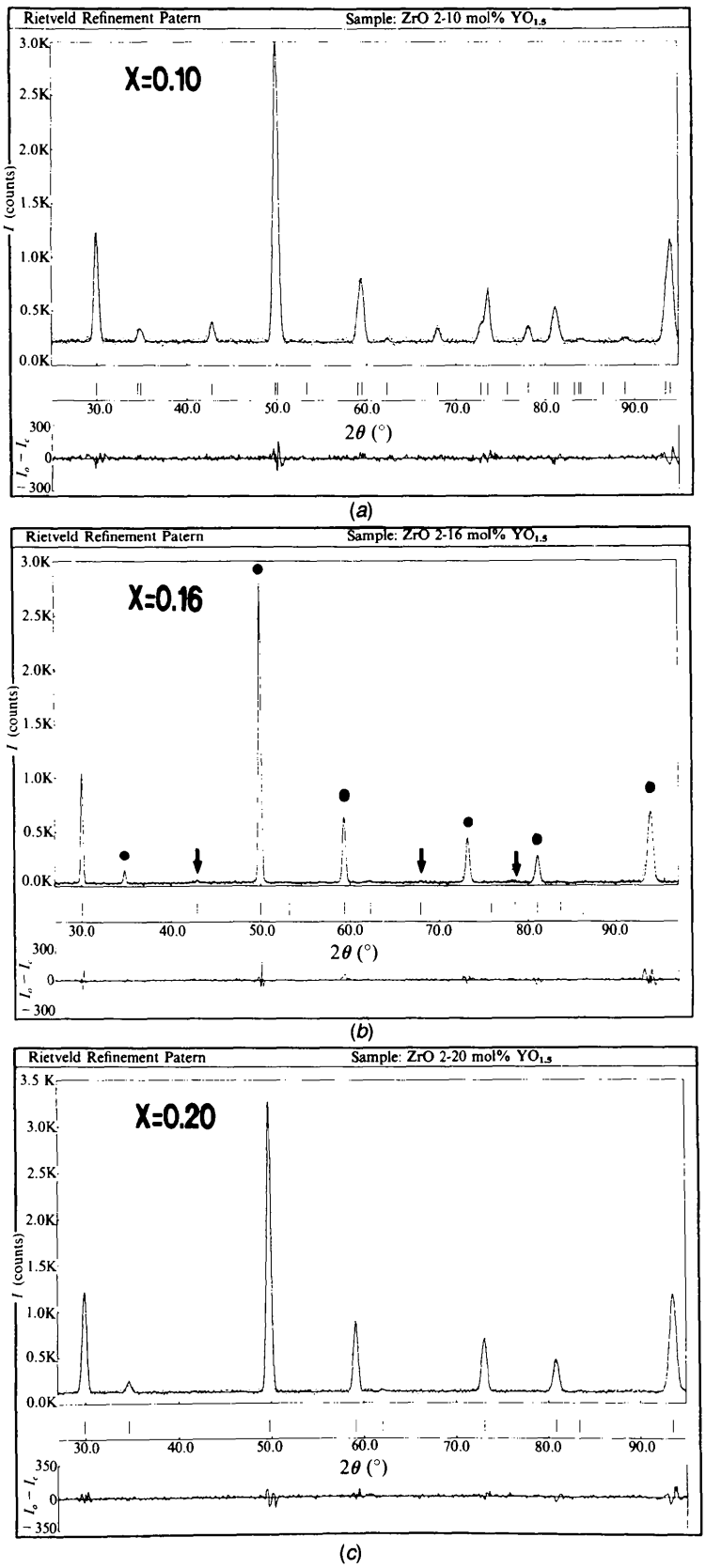

Fig. 7. Observed (dots) and calculated (full line) neutron intensity profiles for (*a*) the *t'* form of $Zr_{0.90}Y_{0.10}O_{1.95}$, (*b*) the *t''* form of $Zr_{0.84}Y_{0.16}O_{1.92}$, and (*c*) the cubic phase of $Zr_{0.80}Y_{0.20}O_{1.90}$.

and Fig. 8). The z values estimated by Rietveld analyses agreed well with those found by direct calculation from the intensity ratio (Fig. 8). Although the 112_f reflection could not be observed at the compositional region of $X \geq 0.18$, the z values can be extrapolated linearly with $YO_{1.5}$ content to $z = 0.25$ where the symmetry changes to cubic (broken line in Fig. 8). The tetragonal–cubic phase boundaries estimated from direct calculation and by the Rietveld analyses with and without the subtraction of the diffuse scattering were around 0.20. The z values for $X = 0.18$ and 0.20 estimated by the Rietveld method, assuming tetragonal symmetry, were deviated to lower values from the extrapolated line (Fig. 8). The deviation must be ascribed to the diffuse scattering at *ca* 43° in 2θ, as observed in Fig. 6. In fact, the z values (● in Fig. 8) obtained by the Rietveld analyses after the subtraction of the diffuse scattering were larger than those (× in Fig. 8) obtained by the Rietveld analyses of raw neutron diffraction data for $X = 0.16$, 0.18 and 0.20. Steele & Fender (1974) reported similar diffuse scattering in ZrO_2–$YO_{1.5}$ solid solutions. These results indicate that the tetragonal phase exists in the compositional region of $X \leq 0.16$ at least and suggest that the phase boundary is located around $X = 0.20$ or a composition larger than $x = 0.20$. For more exact determination of the oxygen position around the phase boundary it is necessary to subtract more exactly the contribution of the diffuse scattering.

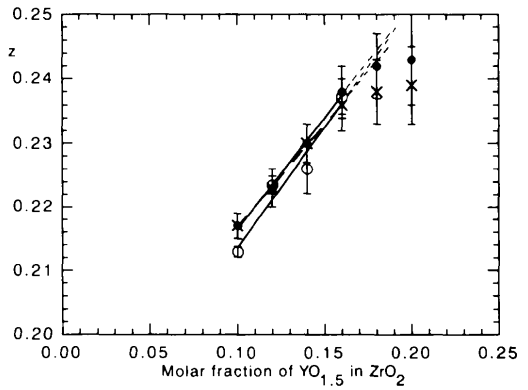

Fig. 8. Variation of the oxygen atomic coordinates against $YO_{1.5}$ contents in ZrO_2 estimated from the integrated intensity ratio (open circle) and the Rietveld refinement (closed circle, X).

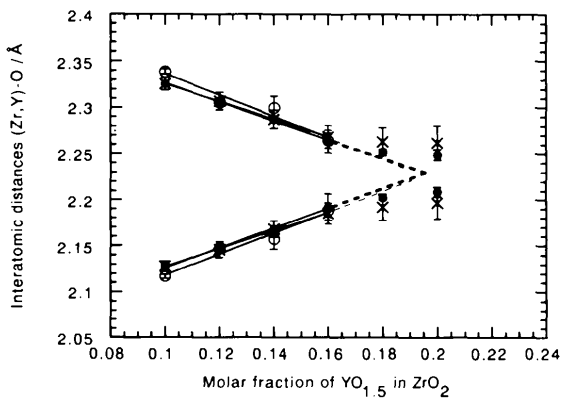

Fig. 9. Variation of the interatomic distances (Zr,Y)—O against $YO_{1.5}$ contents. The interatomic distances (Zr,Y)—O were estimated from the integrated intensity ratio (open circle) and the Rietveld refinement (closed circle, X).

There are two kinds of interatomic distance between cation and anion in the tetragonal structure, r(Zr,Y)—O^+ and r(Zr,Y)—O^-, where r(Zr,Y)—O^+ > r(Zr,Y)—O^-. The values of r(Zr,Y)—O^+ and r(Zr,Y)—O^- approach with an increase of $YO_{1.5}$ content (Fig. 9). The extrapolated lines of r(Zr,Y)—O^+ and r(Zr,Y)—O^- estimated from the direct calculation and by the Rietveld analyses with and without the subtraction of the diffuse scattering coincide with each other around $X = 0.20$.

The atomic coordinate z at lower compositional regions of $X = 0$ and $X = 0.06$ (Teufer, 1962; Aldebert & Traverse, 1985; Michel *et al.*, 1983; Howard, Hill & Reichert, 1988) can be plotted on the curve extrapolated by the present data. Zhou *et al.* (1991) suggested that the 112_f type electron-diffraction intensity and the oxygen displacement decreased with an increase of $YO_{1.5}$ content. However, they could not quantify the degree of displacement. Sato *et al.* (1991) found that the z value increases with an increase of $YO_{1.5}$ content in the compositional region of $0.039 \leq X \leq 0.122$. The present paper reports, for the first time, the compositional dependence of the oxygen displacement from the anion site in the ideal fluorite-type structure around the cubic–tetragonal phase boundary.

There is a report on the coexistence of cubic and tetragonal phases in arc-melted $Zr_{1-x}Y_xO_{2-x/2}$ specimens ($X = 0.13$ and 0.14) and the observation of a cubic single phase in the compositional region of $X \geq 0.15$ (Scott, 1975). Noma, Yoshimura, Sōmiya, Kato, Shibita & Seto (1989) also reported the coexistence of t' and c phases in rapidly quenched $Zr_{1-x}Y_xO_{2-x/2}$ specimens ($0.095 \leq X \leq 0.131$) through X-ray diffraction studies. Sato *et al.* (1991) reported that the sample with the composition $X \geq 0.131$ showed cubic symmetry. However, they did not consider the t'' form where the oxygen ions displace and $a_f = c$. The present work has indicated the formation regions of t', t'' and c forms by neutron diffraction and X-ray diffraction.

This work was supported partly by the Grant-in-Aid Shôrei-kenkyu 05750607 for Fundamental

Research from the Ministry of Education, Science and Culture, Rikogaku-Shinko-Kai at Tokyo Institute of Technology, the Murata Science foundation and the Mitsubishi foundation.

References

ALDEBERT, P. & TRAVERSE, J.-P. (1985). *J. Am. Ceram. Soc.* **68**, 34–40.

BARKER, W. W., BAILEY, F. P. & GARRETT, W. (1973). *J. Solid State Chem.* **7**, 448–453.

FABER, JR, J., MUELLER, M. H. & COOPER, B. R. (1978). *Phys. Rev. B*, **17**, 4884–4888.

FUNAHASHI, T., ITO, Y. & YOSHIZAWA, H. (1991). *Bull. Phys. Soc. Jpn*, **46**, 1003–1009.

HEUER, A. H., CHAIM, R. & LANTERI, V. (1987). *Acta Metall.* **35**, 661–666.

HEUER, A. H., CHAIM, R. & LANTERI, V. (1989). *Advances in Ceramics*, Vol. 24A, *Science and Technology of Zirconia* III, edited by S. SŌMIYA, N. YAMAMOTO & H. YANAGIDA, pp. 3–20. Westerville: American Ceramic Society.

HILLERT, M. & SAKUMA, T. (1991). *Acta Metall. Mater.* **39**, 1111–1115.

HOWARD, C. J., HILL, R. J. & REICHERT, B. E. (1988). *Acta Cryst.* **B44**, 116–120.

IZUMI, F. (1985). *J. Cryst. Soc. Jpn*, **27**, 23.

IZUMI, F. (1993). *The Rietveld Method*, edited by R. A. YOUNG, pp. 236–253. New York: Oxford Univ. Press.

LEFEVRE, J., COLLONGUES, R. & PEREZ Y JORBA, M. (1959). *C. R.* **249**, 2329–2331.

MCCULLOUGH, J. D. & TRUEBLOOD, K. N. (1959). *Acta Cryst.* **12**, 507–511.

MARTIN, U., BOYSEN, H. & FREY, F. (1993). *Acta Cryst.* **B49**, 403–413.

MICHEL, D., MAZEROLLES, L. & PEREZ Y JORBA, M. (1983). *J. Mater. Sci.* **18**, 2618–2628.

MILLER, R. A., SMIALEK, J. L. & GARLICK, R. G. (1981). *Advances in Ceramics*, Vol. 3, *Science and Technology of Zirconia*, edited by A. H. HEUER & L. W. HOBBS, pp. 241–253. Columbus: American Ceramic Society.

NOMA, T., YOSHIMURA, M., SŌMIYA, S., KATO, M., SHIBATA, M. & SETO, H. (1989). In *Advances in Ceramics*, Vol. 24A, *Science and Technology of Zirconia* III, edited by S. SŌMIYA, N. YAMAMOTO & H. YANAGIDA, pp. 377–384. Westerville: American Ceramic Society.

SAKUMA, T. (1993). *Science and Technology of Zirconia*, Vol. V, edited by S. P. S. BADWAL, M. J. BANNISTER & R. H. J. HANNINK, pp. 86–98. Lancaster: Technomic Publishing Co.

SAKURAI, T. (1985). *X-ray Crystal Analyses*, 9th ed. Tokyo: Sho-Ka-Bo.

SATO, H., YASHIMA, M., YOSHIMURA, M. & TORAYA, H. (1991). *Abstracts of Symposium of Basic Science of Ceramics*, p. 201. Tokyo: The Ceramic Society of Japan.

SCOTT, H. G. (1975). *J. Mater. Sci.* **10**, 1527–1735.

SMITH, D. K. & CLINE, C. F. (1962). *J. Am. Ceram. Soc.* **45**, 249–250.

SMITH, D. K. & NEWKIRK, H. (1965). *Acta Cryst.* **18**, 983–991.

STEELE, D. & FENDER, B. E. F. (1974). *J. Phys. C*, **7**, 1–11.

SUBBARAO, E. C. (1981). *Advances in Ceramics*, Vol. 3, *Science and Technology of Zirconia*, edited by A. H. HEUER & L. W. HOBBS, pp. 1–24. Columbus: American Ceramic Society.

SUGIYAMA, M. & KUBO, H. (1986). *J. Ceram. Soc. Jpn*, **94**, 726–731.

SUTO, H., SAKUMA, T., YOSHIKAWA, N. & HIGUCHI, Y. (1987). *J. Jpn Inst. Metals*, **51**, 710–714.

SUZUKI, S., TANAKA, M. & ISHIGAME, M. (1985). *Jpn J. Appl. Phys.* **24**, 401–410.

TEUFER, G. (1962). *Acta Cryst.* **15**, 1187.

TORAYA, H. (1986). *J. Appl. Cryst.* **19**, 440–447.

TORAYA, H. (1993). In *The Rietveld Method*, edited by R. A. YOUNG, pp. 254–275. New York: Oxford Univ. Press.

YASHIMA, M., ISHIZAWA, N. & YOSHIMURA, M. (1993*a*). *J. Am. Ceram. Soc.* **76**, 641–648.

YASHIMA, M., ISHIZAWA, N. & YOSHIMURA, M. (1993*b*). *J. Am. Ceram. Soc.* **76**, 649–656.

YASHIMA, M., ISHIZAWA, N. & YOSHIMURA, M. (1993*c*). *Science and Technology of Zirconia*, Vol. V, edited by S. P. S. BADWAL, M. J. BANNISTER & R. H. J. HANNINK, pp. 125–135. Lancaster: Technomic Publishing.

YASHIMA, M., MORIMOTO, K., ISHIZAWA, N. & YOSHIMURA, M. (1993). *J. Am. Ceram. Soc.* **76**, 1745–1750.

YASHIMA, M., OHTAKE, K., ARASHI, H., KAKIHANA, M. & YOSHIMURA, M. (1993). *Abstracts of the Annual Meeting of the Ceramic Society of Japan*, pp. 378–383. Tokyo: Ceramic Society of Japan.

YASHIMA, M. & YOSHIMURA, M. (1992). *Jpn J. Appl. Phys.* **31**, L1614–L1617.

YOSHIMURA, M. (1988). *Am. Ceram. Soc. Bull.* **67**, 1950–1955.

YOUNG, R. A., PRINCE, E. & SPARKS, R. A. (1982). *J. Appl. Cryst.* **15**, 357–359.

ZHOU, Y., LEI, T. C. & SAKUMA, T. (1991). *J. Am. Ceram. Soc.* **74**, 633–640.